



Cold Spring Harbor Protocols

Single-Molecule Studies Using Magnetic Traps

Timothée Lionnet, Jean-François Allemand, Andrey Revyakin, Terence R. Strick, Omar A. Saleh, David Bensimon and Vincent Croquette

Cold Spring Harb Protoc 2012; doi: 10.1101/pdb.top067488

Email Alerting Service

Receive free email alerts when new articles cite this article - [click here](#).

Subject Categories

Browse articles on similar topics from *Cold Spring Harbor Protocols*.

[DNA Protein Interactions](#) (37 articles)
[Imaging/Microscopy, general](#) (499 articles)

To subscribe to *Cold Spring Harbor Protocols* go to:
<http://cshprotocols.cshlp.org/subscriptions>

Topic Introduction

Single-Molecule Studies Using Magnetic Traps

Timothée Lionnet, Jean-François Allemand, Andrey Revyakin, Terence R. Strick, Omar A. Saleh, David Bensimon, and Vincent Croquette

In recent years, techniques have been developed to study and manipulate single molecules of DNA and other biopolymers. In one such technique, the magnetic trap, a single DNA molecule is bound at one end to a glass surface and at the other to a magnetic microbead. Small magnets, whose position and rotation can be controlled, pull on and rotate the microbead. This provides a simple method to stretch and twist the molecule. The system allows one to apply and measure forces ranging from 10^{-3} to >100 pN. In contrast to other techniques, the force measurement is absolute and does not require calibration of the sensor. In this article, we describe the principle of the magnetic trap, as well as its use in the measurement of the elastic properties of DNA and the study of DNA–protein interactions.

BACKGROUND

During the past decade or so, a number of new techniques have emerged that allow the manipulation of single DNA molecules and other biopolymers (RNA, proteins, etc.). These experiments permit the measurement of the stretching and twisting elasticity of DNA and have consequently revealed the essential role played by DNA's mechanical properties in its interactions with proteins. In this article, we focus on one particular manipulation technique, the magnetic trap. We describe briefly its principle and use in the measurement of the elastic properties of DNA and the study of DNA–protein interactions. We then describe in more detail the protocols commonly used to work with magnetic traps.

When, in 1953, Watson and Crick proposed their famous double-helical structure for DNA (Watson and Crick 1953b), it was already known to be responsible for genetic heredity (Avery et al. 1944; Hershey and Chase 1952). However, Watson and Crick's major discovery significantly changed the thinking about cellular processes such as the replication of DNA (Watson and Crick 1953a) and cell division by providing a much-needed molecular and structural basis. Ever since, it has become clear that the study of DNA's molecular interactions within a cell is necessary to understanding its function. In the 50 years following the discovery of the double helix, numerous techniques emerged that allow one to transform, synthesize, and sequence DNA molecules and also to study and quantify the interactions between biomolecules (e.g., protein–DNA interactions). The climax of this so-called “Genomic Era” was reached when the human genome sequencing program attained its goal.

In parallel, in the past decade or so, biophysicists have developed a variety of single-molecule nano-manipulation techniques (e.g., optical tweezers, atomic force microscopes, and magnetic traps). These methods have been used to monitor the mechanical response to force of different biopolymers, such as double-stranded DNA (dsDNA), single-stranded DNA (ssDNA), RNA, and proteins. They also

Adapted from *Single-Molecule Techniques* (ed. Selvin and Ha). CSHL Press, Cold Spring Harbor, NY, USA, 2008.

© 2012 Cold Spring Harbor Laboratory Press

Cite this article as *Cold Spring Harbor Protoc*; 2012; doi:10.1101/pdb.top067488

developed optical methods based on fluorescence to follow biochemical reactions by observing the signal (position, displacement, intensity) of one single fluorophore.

From a physical standpoint, the study of single-molecule elasticity has provided an ideal testing ground for classic models of polymer elasticity. It has also stimulated theorists to take into account the interactions (electrostatic, base pairing, self-avoiding) present in more realistic polymer chains. From a biochemical and structural standpoint, single-molecule nanomanipulation techniques have made it possible to study protein activity under an applied mechanical stress. Such mechanical stress is common *in vivo*, arising, for instance, in compacted, supercoiled DNA in the cell nucleus, in the rapid intracellular transport of vesicles, or in the activation of mechanically gated ion channels at the cell surface. In particular, single-molecule studies highlighted the importance of tension and torsion at the molecular scale for modulating protein–DNA and protein–protein interactions. Indeed, it is well accepted that proteins perform catalysis by cycling through different structural conformations. These structural rearrangements can be quite large and complex and thus are frequently rate limiting. Applying an assisting or opposing external force to a protein molecule can speed up or slow down the conformational change and hence the catalytic cycle. The protein molecule's response to force gives information on the way in which mechanical deformations are involved in its conformational cycle. Finally, from an enzymological standpoint, and in contrast to bulk assays that measure the average activity of an ensemble of proteins (some of which may be inactive), single-molecule techniques allow the measurement of the distribution of activities of individual enzymes and permit the measurement of the rate, processivity, and step size of single enzymes as a function of force and nucleotide triphosphate (e.g., ATP) concentration. These studies provide detailed information on the rate-limiting steps in the conformational cycle.

In this article, we focus on one particular manipulation technique: the magnetic trap. We briefly sketch its use in the study of DNA molecules under tension and torsion and in the investigation of DNA–protein interactions (topoisomerases, DNA and RNA polymerases, helicases, translocases, etc.). We then sketch how to build a magnetic trap system and describe the typical protocol used to investigate protein–DNA interactions.

PHYSICS OF THE MAGNETIC TRAP

Protein–DNA interactions frequently result in a modification of DNA structure or conformation through bending, stretching, twisting, or modification of base pairing. When such changes occur on a DNA molecule extended by an external stretching force, they often produce a detectable change in the DNA molecule's end-to-end extension. DNA nanomanipulation techniques are used to apply force on a single DNA molecule and subsequently provide a measurement of the molecule's extension with high temporal and spatial resolution.

To monitor enzymatic activity, DNA nanomanipulation must, of course, be performed in an aqueous solution with a defined salt concentration. The best observation technique for such conditions is the optical microscope. Nevertheless, directly visualizing changes in DNA extension is not feasible for two reasons. First, single DNA molecules are too small to efficiently scatter visible light, and so are not visible in conventional light microscopy. In addition, high-resolution fluorescent visualization is relatively difficult to achieve because of diffraction limitations. Second, Brownian fluctuations further smear out the image of the molecule. To overcome the resolution issue, a simple solution is to attach to one end of the DNA molecule a marker large enough to be seen under the optical microscope. To decrease the effect of Brownian fluctuations, we apply a stretching force to the molecule. Both conditions can be satisfied by attaching one end of the molecule to a marker (typically a micron-sized bead) and immobilizing the second end on a solid surface such as a glass coverslip.

To twist and stretch a DNA molecule and study its interactions with proteins, a magnetic trap technique (Strick et al. 1996) has proved particularly convenient (Ali et al. 2001; Danilowicz et al. 2003; Leuba et al. 2003; Dawid et al. 2004; Fulconis et al. 2004; Seidel et al. 2004; Yan et al. 2004; Koster et al. 2005; Gore et al. 2006). Other means can also be used to twist DNA (Friese et al. 1996, 1998; Nieminen

et al. 2001; Bryant et al. 2003; La Porta and Wang 2004), but they are far more complex. Briefly, the magnetic technique consists of stretching a single DNA molecule bound at one end to a glass surface and at the other to a magnetic microbead (0.5–4.5 μm in diameter) (Fig. 1A). Small magnets, whose position and rotation can be controlled, are used to pull on and rotate the microbead and thus stretch and twist the molecule. This system allows one to apply and measure forces ranging from a few femtoNewtons (10^{-3} pN) to >100 pN (Strick et al. 1998) with a relative accuracy of $\sim 10\%$. In contrast to other techniques, this force measurement is absolute and does not require a calibration of the sensor. It is based on the analysis of the Brownian fluctuations of the tethered bead, which is completely equivalent to a damped pendulum of length $l = \langle z \rangle$ pulled by a magnetic force F (along the $\langle z \rangle$ -axis). The pulling force on the bead gives rise to a transverse restoring force, equivalent to a spring with stiffness $k_x = F/\langle z \rangle$ (Yan et al. 2004). In addition to the magnetic force, the bead is subjected to the stochastic Langevin force $F_L(t)$ (responsible for the fluctuations characteristic of the Brownian motion) and to a friction force $F_v = \gamma\eta r$ ($\gamma = 6\pi$ for a sphere of radius r far from a surface; $\eta = 10^{-3}$ MKS is the viscosity of water). The equation of the particle's transverse motion is the following:

$$k_x x(t) + \gamma\eta r \frac{\partial x}{\partial t} = F_L(t)$$

Because the system is overdamped, the inertial term is negligible and has been omitted. The Langevin force can be modeled as a white noise, with the following properties: $\langle F_L(t) \rangle = 0$ and $\langle F_L(t)F_L(t') \rangle = 4k_B T\gamma\eta r\delta(t - t')$. In Fourier space, the equation above translates into (Berg-Sorensen and Flyvbjerg 2004):

$$k_x \tilde{x}(f) + 2\pi\gamma\eta r f \tilde{x}(f) = \tilde{F}_L(f)$$

where f , $\tilde{x}(f)$, and $\tilde{F}_L(f)$ denote, respectively, the frequency and the Fourier transforms of $x(t)$ and $F_L(t)$. Note that because we are dealing with frequency (in Hertz), these formulae change when

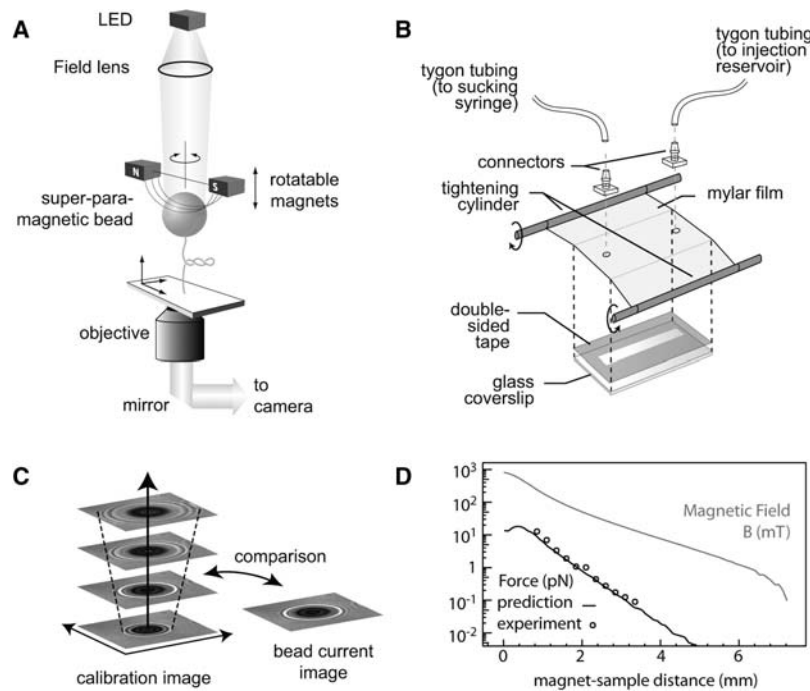


FIGURE 1. Experimental setup. (A) Schematic view of the setup (not to scale). (B) Design of the experimental micro-chamber. (C) Principle of the bead z position measurement. At each time, the current bead image is compared to the calibration image (see text). (D) Experimental measurement of the magnetic field (gray line) created by the magnet setup described in the text. Prediction of the resulting force generated on 1- μm -diameter beads (MyOne, Dynabeads; Invitrogen) using manufacturer's magnetization data (black circles). Force actually measured using the method described in the text on a similar bead (black line).

considering radial frequency ω . In frequency space, the density of transverse fluctuations (i.e., the one-sided power spectrum of the transverse fluctuations [Bracewell 1999]) is then given by:

$$|\tilde{x}(f)|^2 = \frac{4\gamma\eta rk_B T}{k_x^2} \frac{1}{1 + (f/f_c)^2}$$

where $f_c \equiv k_x/(2\pi\gamma\eta r) = F/(12\pi^2\eta r\langle z \rangle)$. This power spectrum is a Lorentzian that is proportional to η and r . By fitting the power spectrum of the fluctuations to a Lorentzian, one obtains two parameters: the integral of the spectrum and the cutoff frequency f_c . The frequency f_c gives the characteristic response time of the system $\tau_b \equiv (2\pi f_c)^{-1}$. The integral of the spectrum is equal to $k_B T\langle z \rangle/F$, which is equivalent to the equipartition theorem (Einstein 1956; Reif 1965). This gives an estimate of F , knowing the mean extension $\langle z \rangle$ of the DNA-tethered bead, without any assumption on η or r , which are difficult to measure accurately.

Because the characteristic response time of the system is τ_b , one must be careful (1) to sample the signal correctly (i.e., to use a signal sampling period $t_s \equiv 1/f_s$ that is small relative to τ_b), and (2) to acquire data for a long enough time T (such that $T \gg \tau_b$). In practice, the sampling period is set by the recording device (in this case, a camera operating at 60 Hz). If $f_s > 4f_c$, the method based on the integral of the spectrum is valid to a few percent. If $f_s < f_c$, the relation is not valid because signal aliasing and data filtering by the camera significantly reduce the bead fluctuations, which results in an overestimation of the force. Accounting for these phenomena is feasible in Fourier space; valid corrections can be applied when $f_s > 2f_c$ (Berg-Sorensen and Flyvbjerg 2004). When fitting the power spectrum, one must also be careful to perform proper data averaging in Fourier space (i.e., “blocking”) (Press et al. 1992; Berg-Sorensen and Flyvbjerg 2004). Overall, a simple rule of thumb states that the relative accuracy of the Brownian measurement is given by $\sqrt{\tau_b/T}$ (Strick et al. 1998).

From the bead’s Brownian fluctuations (δx^2 , δy^2), one can thus extract the force pulling on the DNA molecule (the smaller the fluctuations, the greater F), and from δz^2 , one can obtain the force’s first derivative, $\partial_z F$. This measurement method is valid with magnetic (but not optical) traps because the variation of the trapping gradients occurs on a scale (O [1 mm]) much larger than the scale on which the elasticity of the molecule changes (O [0.1 μm]). In other words, a magnetic trap device is a constant force device (as long as the position of the magnets is fixed). With cantilevers or optical tweezers, working at constant force requires an appropriate feedback system to ensure that the displacement of the sensor (and consequently, the force) is kept constant. However, because the effective stiffness depends on the force, the magnetic trap technique has a slow response time in the low force range ($F < 1$ pN). Consequently, measuring very weak forces is easy but requires a long time.

Finally, the constant-force magnetic trap is not the only possibility offered by the magnetic tweezers: It is possible to implement a constant-position magnetic trap using an electromagnet-based feedback system (Gosse and Croquette 2002), thus turning the magnetic tweezer setup into the equivalent of an optical tweezer (except for the time response of the feedback system). Using either optical tweezers or magnetic tweezers, it is possible to twist a DNA molecule (Friese et al. 1996, 1998; Strick et al. 1996; Leger et al. 1999; Nieminen et al. 2001; Bryant et al. 2003; La Porta and Wang 2004). One advantage of specially designed optical tweezers is that they can directly measure the torque applied to the molecule (La Porta and Wang 2004); this is not possible with a magnetic tweezer. However, whereas twisting DNA with optical tweezers is a rather complex experiment, the magnetic traps achieve this goal with an extremely simple setup: Rotation of the magnetic bead is achieved by rotating the magnets with a motor.

BUILDING A MAGNETIC TRAP: AN OVERVIEW OF THE SETUP

Magnetic Trap Design and Properties

The apparatus consists of an inverted microscope featuring a pair of strong magnets placed just above the sample. Two NdFeB cubic magnets are positioned so that their opposing poles face each other, separated by a gap of 0.5–1 mm. This configuration results in a very strong (~ 1 T), horizontally

oriented magnetic field in the gap separating the magnets. The magnet pair is centered on the (vertical) optical axis, in such a way that the light beam passes through the gap. Outside the gap, but along the optical axis, the magnetic field remains horizontal and decays rapidly with vertical distance from the magnets (Fig. 1D).

The presence of the magnetic field induces a magnetization on a superparamagnetic bead positioned in the sample. The bead's moment is aligned with the magnetic field (i.e., horizontally). However, the magnetic force generated on the bead is oriented along the magnetic field gradient (i.e., vertically upward). Experimentally, we find that the strength of this force decreases roughly exponentially with the vertical distance from the bead to the magnets (Fig. 1D). The characteristic decay length is on the order of the size of the gap between the two magnets, typically 0.5 mm. The magnitude of the force applied on the bead can therefore be varied by vertically translating the magnets. This is achieved using a motorized translation stage (Polytec PI M-126.PD). In a typical nanomanipulation experiment, the bead attached to a DNA molecule may move by a few microns. Over that distance, the stretching force varies by <0.1% and may be considered as constant.

Because of a slight anisotropy in the magnetic properties of the paramagnetic beads, a bead subjected to a magnetic field tends to align itself along a preferred direction, in a fashion similar to a compass needle. Using another motor (Polytec PI C-150.PD), the magnets can be rotated around the optical axis. In this process, the force applied to the bead remains constant, but the bead rotates with the magnetic field direction. The rotation speed can be as high as 10 turns per second. The maximum torque applied by the magnets to the bead varies with the force but is always very strong, on the order of 1000 pN nm. It is so high that the elastic torque applied by DNA is negligible and the bead's magnetic moment will always be perfectly aligned with the magnetic field.

Tracking Bead Position in Three Dimensions with Nanometer Resolution

Most applications of magnetic tweezers require measuring the elongation of the molecule, which corresponds to the vertical position of the bead. A convenient way to do this is to use the features of the diffraction (Talbot) images produced by the bead (Ovryn 2000; Ovryn and Izen 2000). A slightly focused illumination beam generated by a relatively monochromatic source (a superbright LED is a good choice [e.g., Lumiled 625-nm wavelength]) results in an almost parallel illumination of the sample. The illumination comes from above the sample and the observation is performed from below using an oil immersion microscope objective (Olympus 100 \times , numerical aperture [NA] = 1.2). The light collected through the objective is reflected by a dielectric mirror and sent through a 200-mm lens onto a JAI CV-M30 camera operating at 60 Hz (Fig. 1A). The camera signal is then digitized with a frame grabber (Corecco PCVision+). Images are analyzed in real time with a computer.

Under such illumination conditions, the bead image is decorated by a series of diffraction rings whose shapes depend on the relative distance between the bead and the focal plane (Fig. 1C). When the bead is in focus, these rings disappear, but they increase in diameter as the bead moves out of focus. By precisely stepping the focal plane through a series of positions (e.g., by moving the objective with a piezo-electric device), one forms a stack of calibration images that records the shape of the diffraction rings versus distance from the focal plane. Then, custom software (described below) can determine the out-of-focus distance for a new bead image by comparing its diffraction pattern to the calibration stack.

The tracking algorithm (Gosse and Croquette 2002) consists of two steps. First, we determine the x and y coordinates of the center of the bead; then, from that position, we compute the averaged radial intensity profile of the image and use it to determine the z position. The determination of the bead's x and y coordinates is performed independently and relies on two assumptions: first, that the bead is centrosymmetric, and second, that the bead moves at most by a few pixels from one frame to the next. To determine the x position, we extract an intensity profile $I(x)$ that runs along the extent of the bead image and is averaged over a few pixels in y . $I(x)$ is centered on the x position of the bead from the previous frame. We then compute the correlation function $C(x_0) \equiv \int I(x)I(-x + x_0) dx$ using an FFT algorithm. The maximum of $C(x_0)$ occurs at a position δx , which is twice the shift of

the bead's position from the profile center. Typically, a pixel of the camera corresponds to 100 nm, so precise measurement of x requires subpixel resolution, which is achieved by polynomial interpolation and a moderate low-pass filtering. The same procedure is performed to find the center in y .

Knowing the bead's center horizontal position, we compute the image radial profile $I_u(r)$ where the radial coordinate r is measured from the bead's center and $I_u(r)$ is averaged over all angles. This part of the algorithm is simple but involves performing more than 10^4 square-root operations and, therefore, constitutes the most time-consuming step. We exclude the central area of the bead image so that we only consider the diffraction rings of the image [$I_u(r > r_c)$]. The value of r_c is determined empirically to exclude the central part of the image, which displays a complex variation of light intensity with respect to the bead's distance from the focal plane. The diffraction rings can be viewed as a wave packet $I_u(r)$ that we compare in a least-square fashion to the calibration image (corresponding typically to 32 profiles sampled over 10 μm). With this process, we easily identify the closest profile in the calibration image $I_n(r)$. This leads to a coarse estimate (within 0.33 μm) of the bead's z position. To achieve better resolution in z , we interpolate the position of $I_u(r)$ between $I_n(r)$ and $I_{n+1}(r)$ in the calibration image. This is achieved by measuring the phase difference between the wave packets. To extract the phase, we take the Hilbert transform of the radial profile. We have found that the phase difference between radial profiles varies almost linearly with the z position. The algorithm execution time depends on the square of the number of points N in the profiles. For $N = 128$, the execution time is 1 msec. This can be decreased by a factor of three using SIMD (single instruction multiple data) instructions (Pentium IV at 3 GHz).

This tracking method has some limitations: It only allows bead tracking in a limited range of vertical positions (i.e., the size of the calibration image, typically 10 μm) and restricts the recording of the bead's motion to one side of the focal plane. However, it offers a remarkable accuracy: For a 1- μm -diameter bead immobilized on a surface imaged at 60 Hz, the uncertainty of the tracking algorithm is typically ~ 1 nm in the x , y , and z directions. In an unzipping configuration (i.e., when the two strands of a DNA molecule are pulled apart), this accuracy corresponds to the opening of 2 bp. However, in many situations, the experimental noise is dominated by the Brownian motion of the bead attached to the molecule. To reduce this noise, one can alternatively increase the applied force, reduce the size of the DNA molecule used, or reduce the size of the bead.



Beyond the Drift: Increasing the Apparatus's Possibilities

The enzymes studied typically generate extension changes on a DNA molecule in the range of a few tens of nanometers, during bursts lasting for a few seconds separated by minutes of inactivity. Unfortunately, commercial microscopes have not been designed for such a purpose, and they display a slow drift. This drift is mostly induced by the thermal expansion of the microscope components on variations in the temperature of the environment. We have measured that the focal position of a microscope objective alone drifts by typically a micron per degree of temperature change. Thus, a 0.01 $^{\circ}\text{C}$ temperature variation results in a 10-nm change in the recorded DNA extension!

A simple way to overcome this issue is to perform differential measurement, i.e., to measure continuously both the position of the bead of interest and the position of a bead fixed on the microchamber surface. Some magnetic beads might nonspecifically bind to the surface and be used for that purpose. Alternatively, one can bind nonmagnetic beads onto the surface using simple protocols (see below and **Magnetic Trap Construction** [Lionnet et al. 2012]). Subtracting the two traces of bead position removes most of the drift from the apparatus. Because most of the thermal drift occurs in the low time-frequency domain, the high-frequency part of the fixed bead time trace is mostly composed of tracking noise and low-amplitude Brownian motion (if the fixed bead is not perfectly immobile). Therefore, to avoid adding up unnecessary noise, the fixed bead time trace should be low-pass-filtered before subtraction.

Differential measurement alone is not a perfect solution. First, thermal drift might occur during the recording of the calibration image of a given bead, thus affecting all subsequent measurements on this bead. Second, thermal drift during long acquisition times can easily outrange the size of the

calibration image and result in tracking failure. As a consequence, experiments are made much easier by using a temperature-regulated microscope or, even better, a carefully designed microscope where thermal expansions of the different components are matched so that they almost compensate each other.

DNA PREPARATION AND ANCHORING

Molecular Anchoring, A Prerequisite for Manipulation

The first step in any DNA manipulation experiment is to anchor the DNA molecule (preferentially via its extremities) to appropriately treated surfaces. Many different methods have been developed to achieve specific DNA binding to surfaces. They have found useful applications, from gene mapping, sequencing, and analysis (Chee et al. 1996) to the development of very sensitive immunological assays (immuno-PCR [polymerase chain reaction]) (Sano et al. 1992). A first method, which does not require any modification of the molecule, relies on the specific adsorption of DNA by its ends onto hydrophobic surfaces at a pH of about 5.5 (Allemant et al. 1997). DNA has been observed to adhere strongly and nonspecifically at low pH and weakly or not at all at high pH on various hydrophobic materials (Teflon, polystyrene, graphite, silanized glass). Between these two regimes, there exists a narrow pH range ($\text{pH} = 5.5 \pm 0.2$) where DNA binds to the surface by its extremities only. Surprisingly, once the DNA has bound to the surface, it remains anchored even when the pH is altered. That method has been used to anchor and pull on DNA with optical tweezers (Shivashankar et al. 1999).

A second method exploits the fact that modified DNA molecules with extremities bearing reactive groups (e.g., primary or secondary amines, carboxyl or thiol moieties) can be anchored to the corresponding surface (e.g., carboxyl, amine, or gold) (Lee et al. 1994; Yang et al. 1998). Similarly, surfaces coated with oligonucleotides can be used to recognize a complementary extremity on the DNA molecule of interest. However, most of the applications achieve the required binding specificity via biochemical reactions between a DNA molecule that has been end-labeled with a functional group (biotin, fluorescein, digoxigenin) and a surface appropriately coated (e.g., with streptavidin to bind biotin or with an antibody against fluorescein, digoxigenin, etc. [Smith et al. 1992]). In addition, if one wishes to twist DNA, each extremity of the molecule must be anchored to the appropriate surface via multiple linkages. The protocol **Magnetic Trap Construction** (Lionnet et al. 2012) describes a simple way to achieve DNA end-labeling. Note that other ways of end-labeling DNA exist and that the molecules are not specifically designed for magnetic tweezers experiments and may be used for any nanomanipulation purpose. The same constructs can be used, for example, with optical tweezers.

Surface Functionalization

Most of the magnetic beads used in magnetic tweezers experiments can be easily purchased with a streptavidin coating and are thus ready to use. We describe in this article, a method for coating the surface with antidig, an antibody against digoxigenin (dig). However, different protocols can be used successfully. Some rely on a chemical reaction with a functionalized glass surface and amino or carboxyl groups of the antibody. A simple and efficient way relies on the adsorption of the antibody to a hydrophobic surface (as in ELISA). Regardless of the protocol used, the binding of antibody to the surface must be followed by a passivation step to limit the nonspecific interactions between the surface and the DNA, proteins, and beads. Although different methods exist (Revyakin et al. 2003), the protocol **Magnetic Trap Construction** (Lionnet et al. 2012) has been used successfully in the study of DNA elasticity (Lionnet et al. 2006) and DNA–protein interactions (Saleh et al. 2005).

Microchamber Design

The use of the smallest possible microchamber is recommended for two reasons. First, it reduces the experimental volume. Second, a thin chamber allows the magnets to be brought close to the sample ($\sim 100 \mu\text{m}$), which results in a high magnetic field gradient inside the sample. This way, one can either

apply high forces on given beads or, if high forces are not required, use smaller beads. This decreases the Brownian fluctuations of the beads and therefore increases both the signal-to-noise ratio and the characteristic response time of the bead–DNA system. The details for constructing a microchamber suitable for magnetic tweezers experiments, including the antibody binding and passivation steps, can be found in **Magnetic Trap Construction** (Lionnet et al. 2012). Using this configuration, the minimum distance from the magnets to the sample can be as small as 100 μm . This allows the application of 15-pN forces on 1- μm -diameter beads (MyOne, Dynabeads; Invitrogen).

Surface Treatment

Before forming the microchamber, the glass coverslip is rendered hydrophobic by allowing it to react with a solution of a chlorinated organopolysiloxane in heptane (Sigmacote; Sigma-Aldrich). The hydrophobic glass coverslip is then incorporated in the microchamber. The antidig coating of the surface is achieved by incubating the microchamber with a solution containing antidig. Finally, the surface is passivated against nonspecific interactions by incubating a passivation solution in the chamber for typically 2–4 h.

Guidelines for DNA Preparation

The first step is to choose the DNA sequence of interest, whose length can range from a few tens of base pairs to a few tens of kilobases. Typically, this central DNA fragment is a sequence contained in a plasmid between two restriction sites. A sufficient amount of DNA (1 d of single-molecule experiments typically requires a few microliters of a 10–100 pM DNA solution) is prepared either via a mini-prep or via a PCR of the region containing the central DNA fragment and a restriction site on each end. The DNA is then cut at both restriction sites, and the region containing the central DNA fragment is isolated from the restriction by-products (using gel extraction—care should be taken to minimize UV-light-induced DNA damage—or a purification column). The restriction enzymes used should leave cohesive ends, with overhangs as long and GC-rich as possible, to increase the yield of the subsequent ligation reaction.

To be manipulated, the central DNA fragment must be flanked by two anchoring DNA fragments. These should be a few hundred base pairs long. Each anchoring fragment must include one restriction site leaving a cohesive end complementary to one of the ends generated on the central DNA fragment. There is no additional sequence requirement other than the absence of any sequence interfering with the activity of the proteins to be studied. Anchoring fragments are generated by two separate PCRs. The labeling is achieved by adding to the standard dNTPs in each PCR a fraction of the suitably labeled dUTP (respectively, digoxigenin-dUTP or biotin-dUTP). The ratio of labeled nucleotide to standard nucleotide is typically on the order of 1:10 to 1:4. The PCR products are then purified using standard protocols to remove the residual primers and other PCR reagents. The final step is the ligation of the anchoring fragments to the central DNA fragment using DNA ligase, thanks to compatible cohesive sites generated by the restriction enzymes. To increase the yield of the ligation, an excess of anchoring fragments (e.g., four- to tenfold) is recommended to saturate the central fragment with labeled handles.

The resulting DNA product is mixed first with the magnetic beads in a test tube, with a typical ratio of 10 beads per DNA molecule (one should use a smaller ratio when two DNAs per bead are wanted, e.g., for DNA-braiding experiments). This ensures that, statistically, each bead will be bound to at most one DNA molecule. After a brief incubation, the bead–DNA mixture is injected in the tweezer setup. In the absence of a magnetic force, the beads are allowed to sediment on the antidig-coated glass surface for a few minutes. The free beads are rinsed away by a gentle hydrodynamic flow. Finally, the magnetic force is applied, and one can browse the surface for a tethered magnetic bead. A more detailed protocol may be found in **Magnetic Trap Construction** (Lionnet et al. 2012) and in Revyakin et al. (2005).

Some tricks can be used whenever possible, even though they are not compulsory. To limit the effect of any interference between restriction enzymes and labeled bases, one can either use a

restriction site containing only Gs and Cs or simply position the site within the PCR primer. To limit the number of unwanted by-products after ligation, nonpalindromic enzymes (which generate fragments that cannot be ligated to themselves) can be selected. Complete purification of the final ligation products (e.g., from biotin–biotin fragments resulting from the ligation of biotin handles on themselves when using palindromic restriction enzymes) is usually unnecessary, as only the DNA products containing both digoxigenin and biotin ends will specifically bind to the bead and surface.

A Variety of DNA Substrates Can Be Used in Magnetic Traps

In the cell, some enzymes are active on dsDNA without a specific sequence requirement (e.g., topoisomerases, which only need a specific supercoiling state). However, many enzymes interacting with DNA only recognize very specific DNA sequences or substrates. For example, RNA polymerases bind specifically to a promoter sequence at the beginning of a gene, and DNA polymerases bind to a junction between ssDNA and dsDNA. Helicases, on the other hand, separate the two strands of a dsDNA molecule, forming a forked structure. DNA recombination involves a four-way junction intermediate, the so-called Holliday junction. All of these situations may be studied using magnetic tweezers. In the following, we describe briefly how such substrates can be prepared.

The dsDNA Template

This is the template that we have described so far. It is multiply labeled with biotin at one extremity and dig at the other one. Although a single biotin (and respectively, dig) can be used to pull on a single molecule, multiple biotin and dig labeling is required to torsionally constrain the molecule. Moreover, such labeling ensures a stronger binding to the surface and thus a longer lifetime of the anchored DNA molecules.

The choice of the central DNA fragment is crucial in the case of enzymes that recognize a specific DNA sequence. Using the correct sequence, one can study DNA looping enzymes; for instance, those involved in gene regulation (LacI or GalR [Lia et al. 2003]) or DNA excision (CRE). A carefully designed central DNA fragment might even allow the generation of more subtle substrates: If the central sequence has a long palindromic insert, a Holliday junction can be produced when negative supercoiling is induced in the molecule. For detailed descriptions of the preparation of such DNA molecules, see Amit et al. (2004) and Dawid et al. (2004).

The ssDNA Template

The preparation of an ssDNA substrate suitable for a nanomanipulation experiment usually starts from a dsDNA solution (prepared as described above). Before the single-molecule experiment, the DNA is heat-denatured (typically for 5 min at 95°C) and then rapidly diluted in an ice-chilled solution. This process limits the rehybridization of the single strands generated by the denaturation step. The resulting solution is then mixed with magnetic beads and injected into the tweezers setup. The use of an ssDNA substrate is usually cumbersome, because it is more prone to nonspecific interactions than dsDNA. Note also that this method does not allow the investigator to know which of the two denatured strands is attached to the bead under study.

Two dsDNA Molecules Crossing with a Well-Defined Geometry

If one increases the DNA:bead ratio in the mixture used for the tweezers experiments, the probability that two DNA molecules bind to a single bead increases. Although this is a situation that one usually wants to avoid, it can be useful in the study of DNA crossings. When two dsDNA molecules bind a magnetic bead, they are usually separated by some distance, and it is then possible to rotate the bead and to cross the two molecules with a well-defined angle. With a single turn, the two molecules present a single crossing. With multiple turns, the two molecules are braided. Obviously, the binding geometry is not controlled by the investigator, and therefore, the distances separating the anchoring

sites of the two molecules on the bead and glass surface are not known a priori. However, by measuring the extension of this construction as a function of the twist exerted on the molecule, one can deduce a posteriori the geometric parameters of the configuration. This substrate is ideal for studying type II topoisomerases (Charvin et al. 2003, 2005b).

STRETCHING DNA

Once a magnetic bead has been anchored to a surface, it is best to first test whether it is bound by a single DNA molecule. As the magnets are brought into proximity (i.e., within a few millimeters) of the sample, a given bead may show one of three possible scenarios:

1. The bead remains stuck to the surface, because of nonspecific interactions. Such beads can be used as reporters of the drift of the anchoring surface. By performing a differential measurement (i.e., measuring the relative position of a DNA-tethered bead of interest relative to the position of a stuck bead), one can remove the drift from the measurement.
2. The bead is not bound to the surface; the bead flies away from the surface because of the magnetic attraction.
3. If the bead is anchored by DNA molecule(s) to the surface and attracted by the magnets, it hovers at a distance from the surface.

Only those beads fluctuating at a distance from the surface are potentially interesting, as they may be bound by one or more DNA molecules. The next step, therefore, is to check that the bead is anchored by a single DNA molecule. A quick test is to pull the bead with a rather large force (2–3 pN) and rotate the magnets by many turns (50–100). If the bead is tethered by more than one DNA molecule, the anchoring molecules will be braided and the distance of the bead to the surface will decrease. The change in extension is similar whether the molecules are braided clockwise or counterclockwise. On the other hand, if the bead is anchored by a single DNA molecule (in particular if it is nicked), its distance will remain unchanged (if the DNA is unnicked, there might be a slight asymmetric change in extension, upon positive or negative rotation, because of structural transitions in the DNA molecule under twist; see below).

A more precise check of the anchoring of a bead by a single DNA requires a measurement of the elastic response of the molecule to a varying force ($0 < F < 10$ pN). In that regime, the elasticity of a single DNA molecule is very well fit (Smith et al. 1992) by the entropic elasticity of an ideal polymer chain, the so-called worm-like-chain model (Fig. 2) (Bustamante et al. 1994; Marko and Siggia 1995). Without delving into theoretical details, we must mention that there exists a useful analytical formula that satisfactorily approximates the variation of the DNA's relative extension l/l_0 (where l_0 denotes the molecular contour length) as a function of the force F (Bouchiat et al. 1999):

$$\frac{F\xi}{k_B T} = \frac{l}{l_0} - \frac{1}{4} + \frac{1}{4(l - l/l_0)^2} + \sum_{i=2}^7 (l/l_0)^i$$

with $a_2 = -0.5164228$, $a_3 = -2.737418$, $a_4 = 16.07497$, $a_5 = -38.87607$, $a_6 = 39.49944$, $a_7 = -14.17718$, and where $\xi = 50$ nm is the DNA persistence length under physiological salt conditions.

TWISTING DNA

Most polymers are insensitive to torsion because their monomers are linked by single covalent bonds about which the monomers are free to rotate. This property is lost when the polymer possesses no single covalent bond about which torsion can be relaxed. This is the case of the double-helical structure of a DNA molecule with no nicks (i.e., no breaks in one of the strands). This particular feature has very important biological implications. First, from a structural point of view, twisting provides an

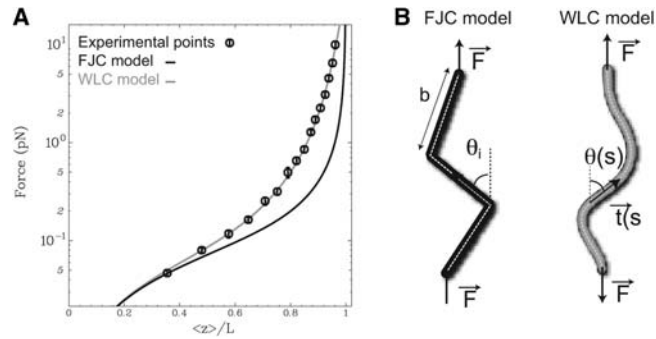


FIGURE 2. Force vs. extension for dsDNA and polymer models for DNA. (A) Experimental force extension curve for one dsDNA molecule (λ -DNA, 16 μm long; black circles). The fit using the worm-like chain (WLC) model (gray line) yields $\xi = 51.6$ nm and $L_0 = 15.6$ μm . The plot of the alternative freely jointed chain (FJC; black line) model using the same value of ξ displays an obvious discrepancy with the experimental data. (B) Principles of polymer modeling by the FJC and WLC models. (Adapted from Charvin et al. 2004.)

efficient way to compact the DNA molecule so that it fits into the cell nucleus, which may explain why in vivo all DNA molecules are twisted. Second, a negatively twisted (underwound) DNA can locally denature (i.e., the two strands locally open). This eases the access to the genetic information normally “hidden” inside the double helix. The local opening of the double helix therefore facilitates DNA interactions with a variety of proteins (RNA polymerases, regulatory factors, etc.). On the other hand, the double-helical structure of positively twisted DNA is more stable at high temperature (i.e., it denatures less). Thus, thermophilic bacteria that live close to the boiling point of water have enzymes that overwind DNA (reverse gyrases). Because the topology of DNA has such an essential role in the cell life, Nature has evolved a family of enzymes, known generally as topoisomerases (the reverse gyrase is one of them), that control the torsion and entanglement of DNA molecules.

The ease with which DNA can be twisted in a magnetic trap setup by simply rotating the magnets makes this system the best choice for the study of coiled (and braided) DNA and its interactions with proteins (e.g., topoisomerases). Although our purpose here is not to dwell on the theory of twisted polymers, much of the experimental response of DNA under torsion can be intuited from our daily experience with twisted cords or tubes pulled by a force F . When one begins to twist such a tube, its extension initially remains unchanged and the constraint is stored as pure torsion. The tube’s torque Γ increases linearly with the twist angle Ω : $\Gamma = (C/l_0) \Omega$, and its twist energy increases quadratically: $E_{\text{torsion}} = (1/2)(C/l_0)\Omega^2$, where C is the tube’s twist stiffness (usually written in the DNA context in units of $k_B T$: $C \equiv k_B T C'$). As one continues to twist the tube, one notices that after a certain number of turns n_b (corresponding to a torque Γ_b), the system buckles and a loop of radius R is formed. The twist energy is thus transferred into bending energy. On further twisting, the tube coils on itself, but the torque no longer increases (Fig. 3B). As a result, the system’s extension decreases by $2\pi R$ for every turn despite the stretching force F . Balancing the torsional energy against the work performed and the increase in bending energy, one gets:

$$2\pi\Gamma_b = 2\pi R F + 2\pi R \frac{B}{2R^2}$$

The radius that minimizes the bending energy is given by $R = \sqrt{B/2F}$, so that $\Gamma_b = \sqrt{2BF}$, $n_b = L\sqrt{2BF}/(2\pi C)$. Thus, the greater the force, the larger the critical buckling torque Γ_b and the number of turns n_b , and the smaller the radius of the loop. On further twisting, the tube coils around itself, but the torque Γ no longer increases. This simple model describes at least qualitatively the behavior of DNA under torsion. The buckling transition is not as sharp as expected for a macroscopic transition because of thermal fluctuations, but increasing the force tends to make the transition sharper. Additionally, past the buckling transition, the DNA’s extension decreases linearly with the number of turns as more coils are added to the molecule without significantly affecting its torque.

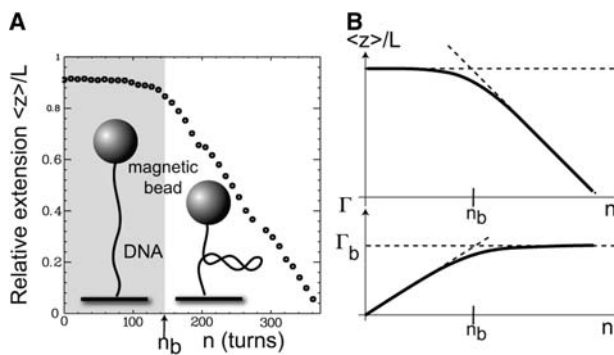


FIGURE 3. Extension vs. supercoiling for one dsDNA. (A) Experimental curve (black squares) shows the normalized extension vs. σ behavior of one single DNA molecule (50 kb) at $F = 1.2$ pN. We distinguish two regimes: At low n , the change in DNA extension is small, while the molecule stores torsional energy. At $n = n_b \approx 140$, the molecule buckles and starts forming plectonemes. After the buckling, the extension decreases almost linearly with the addition of further twisting. (B) As can be understood for an elastic rubber tube, initial twisting does not change the system's extension, but the torque stored in the tube increases linearly with the number of turns n applied. At a given $n = n_b$, forming a loop (plectonemes) costs less energy than increasing the torsional energy. Each additional turn leads to the formation of another loop, so that the extension decreases linearly with n , but the torque $\Gamma = \Gamma_b$ remains constant. (Adapted from Charvin et al. 2004.)

With increasing tension in the DNA, the critical torque for buckling increases. It may be so large that the double helix will respond to the increasing torque not by buckling, but by modifying its internal structure. Two types of structural transitions have been observed. At negative torques ($\Gamma_d \sim -9$ pN nm [Strick et al. 1999; Bryant et al. 2003]), the DNA denatures. Positive torque induces (at a critical torque $\langle \Gamma_p \sim 34$ pN nm [Bryant et al. 2003]) the local formation of a novel structure of DNA called *P*-DNA (Allemand et al. 1998), with a much smaller pitch than *B*-DNA (~ 2.6 bp per turn). This structure is characterized by winding of the phosphate backbone at the center of the helix and exposure of the bases to the solution.

A simple topological formalism summarizes the above discussion. DNA topology is commonly described by three parameters: the twist Tw , the writhe Wr , and the linking number Lk . Twist measures the total number of times the two strands wind about each other, which in regular unstrained *B*-form DNA corresponds to a unit of twist for every 10.5 bp. Writhe measures the total number of self-crossings in plectonemic DNA. The linking number is the sum of twist and writhe: $Lk = Tw + Wr$. For topologically constrained DNA, Lk is a constant and its redistribution between Tw and Wr deformation depends on the buckling torque. After the buckling transition, under physiological conditions of pH (~ 8), salt (~ 150 mM), temperature ($\sim 37^\circ\text{C}$), force (~ 0.5 pN), and supercoiling ($\sim 5\%$), a unit change in Wr will cause a large, $\delta \sim 50$ nm, change in DNA extension. As Tw and Wr deformations are coupled at fixed Lk , a change in Tw in the DNA is accompanied by the formation of an oppositely signed Wr of equal value. As a unit change of Wr causes a large change in DNA extension, a unit change in Tw covering only ~ 10 bp (or ~ 3 nm) of DNA will nevertheless result in an ~ 50 -nm change in DNA extension.

USING MAGNETIC TRAPS TO MONITOR DNA-PROTEIN INTERACTIONS

Magnetic traps have been used to study the interaction of proteins with one or two DNA molecules under fixed force and a given degree of twisting or braiding. Essentially, in all these experiments, one monitors in real time the changes in the DNA extension (the distance of the bead to the surface) as proteins interact with DNA. These changes may be caused by bending or twisting of the molecule (e.g., TopoIV in the absence of ATP [Charvin et al. 2005a]), to the formation of a DNA loop (Lia et al. 2003), to translocation of the DNA (Smith et al. 2001; Dawid et al. 2004; Saleh et al. 2004; Lia et al. 2006), to relaxation of supercoils or braids (Strick et al. 2000; Charvin et al. 2005b; Koster

et al. 2005), to the unwinding of DNA (Dessinges et al. 2004), to the synthesis of a new DNA strand (Maier et al. 2000), etc.

Particularly noteworthy is the recent use of magnetic traps for the mechanistic study of bacterial RNA polymerase (RNAP) (Revyakin et al. 2005, 2006). When RNAP binds to promoter DNA at the beginning of a gene, it reversibly unwinds ~ 13 bp of DNA (a little more than one turn of the double helix) to form an RNAP–promoter open complex (RPO). When this occurs on a negatively supercoiled DNA molecule held in a magnetic trap setup (see Fig. 4A–C), melting is accompanied by the removal of one negative supercoil, resulting in an increase in the extension of the stretched molecule of ~ 60 nm. If the DNA is positively supercoiled, promoter melting is accompanied by the addition of a positive supercoil, resulting in a decrease in the extension of the stretched DNA molecule of ~ 60 nm (see Fig. 4B and D). These relative changes in DNA extension are readily detectable, and it is possible to measure real-time changes in DNA unwinding with single-base resolution by signal averaging over an ~ 1 -sec timescale. Moreover, systematic differences between the change in DNA extension observed on positively or negatively supercoiled DNA can be attributed to DNA bending, which accompanies the formation of an open complex and can also be determined in this analysis.

Figure 5 shows the reversible unwinding of the consensus *lac* promoter under conditions of positive supercoiling. When DNA is in the low-extension position, promoter DNA is unwound by RNAP (RPO). In the high-extension position, promoter DNA is in its native state, but it may be free of RNAP or occupied by an RNAP molecule in the RNAP–promoter closed complex (RPC). The characteristic telegraphic signal obtained provides both structural and kinetic information on promoter unwinding

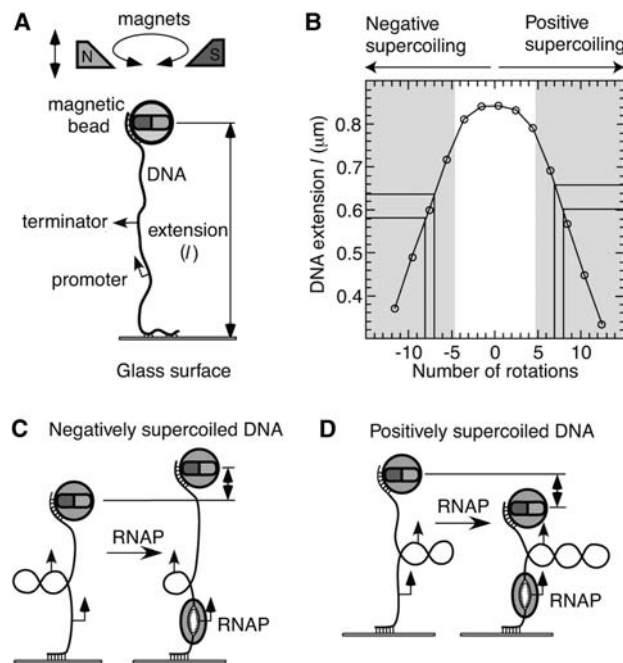


FIGURE 4. Principle of detection of promoter unwinding by a single RNAP molecule. (A) A linear, 2-kb DNA, containing a single bacterial promoter site, a transcribed region, and a transcription termination sequence, is torsionally constrained between a glass surface and a small magnetic bead. The force and rotation applied to the nanomanipulated DNA is controlled by translating and rotating the magnets located above the sample. The resulting DNA's end-to-end extension is determined by measuring the position of the bead above the surface. (B) Extension vs. supercoiling curve obtained for a low stretching force ($F = 0.3$ pN) in transcription buffer (ionic strength 150 mM) at 34°C . Once plectonemes have formed along the DNA, its extension changes linearly at a rate $\delta = 56$ nm for a unit change of positive or negative supercoiling. (C) For negatively supercoiled DNA, promoter unwinding by RNA polymerase results in the removal of a negative supercoil and an increase in DNA extension. Negative torque will drive the reaction toward the open-promoter state. (D) For positively supercoiled DNA, promoter unwinding causes the formation of a positive supercoil and a decrease in DNA extension. Positive torque will drive the reaction toward the closed-promoter state.

by RNAP. The change in DNA extension is proportional to the number of unwound bases in RPo, and single-base resolution can be obtained with second-scale signal averaging; here, ~ 13 bp are unwound in the open-promoter complex. The waiting time T_{wait} reflects the formation of RPo from free components in a simple Michaelis–Menten scheme involving a binding constant ($K_B \sim 100 \text{ nM}^{-1}$) and a forward rate-limiting step ($k_f \sim 0.3 \text{ sec}$). The lifetime of RPo relates to its thermodynamic stability ($k_r \sim 0.03 \text{ sec}$ for positively supercoiled DNA extended by a 0.3 pN force). Together, these parameters provide an excellent series of benchmarks for determining the effect of a range of molecules (polyanions, antibiotics, effector nucleotides, initiating nucleotides, transcription factors, etc.) on promoter unwinding.

The magnetic trap assay has also been used to characterize subsequent stages of gene transcription by RNA and, in particular, the mechanism by which RNAP escapes from the promoter during the initial stage of transcription. In the presence of all four nucleotides (ATP, UTP, GTP, CTP), RNAP forms RPo and subsequently initiates transcription. However, during transcription of the first 10–15 nucleotides, RNAP remains bound at promoter DNA, a result of the exceptional stability of RPo. Instead of moving along the DNA, RNAP initially reels in and unwinds downstream DNA to transcribe it. This “scrunching” of DNA by initiating RNAP is observed as an abrupt, transient increase in the extent of DNA unwinding following formation of RPo (Fig. 5B). It involves unwinding of about one extra turn of the double helix.

Complementary single-molecule FRET (fluorescence resonance energy transfer) experiments confirm that downstream DNA moves toward the RNAP during this process, which therefore combines untwisting and reeling-in of downstream DNA. Thus, the RNAP–promoter complex is energized during initial transcription as an extra 10 bp or so of DNA are unwound and reeled in during initial polymerization of RNA. This energy ($\sim 16 \text{ kcal/mol}$) accumulated in the stressed intermediate is enough to release the RNAP from the stable open promoter so that it may transcribe the gene. Kinetic analysis of this transient “stressed intermediate” (lifetime $\sim 5 \text{ sec}$) shows that essentially all promoter escape events are preceded by the formation of the scrunched intermediate.

On escaping from the promoter, the transcription bubble is seen to shrink. Thereafter, RNAP moves along the DNA at a rate $V_{\text{max}} \sim 25$ nucleotides/sec, transcribing and propagating with it the transcription “bubble,” in which now only ~ 9 bp are unwound. Finally, on reaching the transcription termination sequence, the bubble closes definitively, indicating the release from the DNA of both full-length RNA and RNAP. Simultaneous structure–function analyses of transcription initiation,

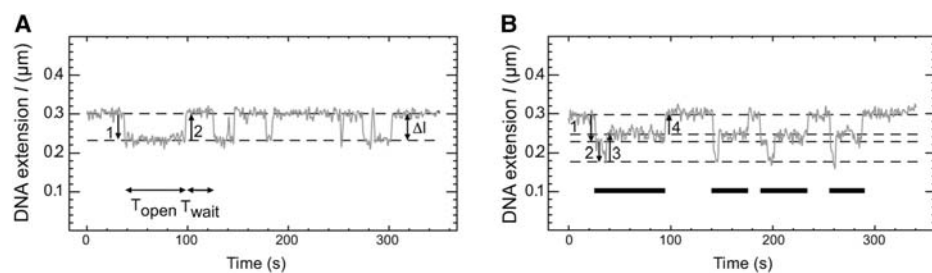


FIGURE 5. Real-time detection of RNAP–DNA interactions. (A) In the absence of nucleotides, reversible unwinding of positively supercoiled T5 N25 promoter appears as a telegraphic signal in the DNA extension. The amplitude of the change in DNA extension Δl_{unwind} is related to the number of unwound bases n as $n = \Delta l_{\text{unwind}} \times 10.5/56$. The duration of a promoter unwinding event T_{unwound} is the inverse of the dissociation rate $T_{\text{unwound}} = 1/k_{\text{off}}$, and is a robust measurement of the thermodynamic stability of the open promoter complex. The waiting time between successive unwinding events T_{wait} is the inverse of the rate of formation of the open promoter complex, $k_{\text{open}} = [\text{RNAP}]k_f / ([\text{RNAP}] + K_B)$. Titration of [RNAP] yields $K_B \sim 100 \text{ nM}^{-1}$ and $k_f \sim 1 \text{ sec}$. (B) In the presence of nucleotides, RNAP progresses through promoter unwinding (transition 1), initial transcription (transition 2), promoter escape (transition 3), productive elongation (from transitions 3 to 4), and transcription termination (transition 4). Initial transcription (from transitions 2 to 3) is accompanied by a large increase in DNA unwinding (~ 10 bp). This transient unwinding of DNA (“scrunching”) has a 5-sec lifetime and always precedes promoter escape. Nucleotide hydrolysis is energetically responsible for this transient increase in unwinding, energizing the complex so that RNAP may break its bonds with the promoter.

promoter escape, productive transcription, and transcription termination provide robust metrics for which to perform comparative analysis of the effects of inhibitors or activators of transcription.

ACKNOWLEDGMENTS

We acknowledge helpful discussions with K.C. Neumann, G. Lia, G. Charvin, E. Praly, and A. Meglio. We thank G. Charvin for help with figure design, and S. Bigot and F.-X. Barre for help in DNA substrate preparation. This work was supported by the Centre National de la Recherche Scientifique, the Dynamique et Réactivité des Assemblages Biologiques, the Ecole Normale Supérieure, and Universities Paris VII and VI and by grants from Association pour la Recherche contre le Cancer, Agence Nationale de la Recherche, and the European Union (Biosense).

REFERENCES

- Ali BM, Amit R, Braslavsky I, Oppenheim AB, Gileadi O, Stavans J. 2001. Compaction of single DNA molecules induced by binding of integration host factor (IHF). *Proc Natl Acad Sci* **98**: 10658–10663.
- Allemand J-F, Bensimon D, Jullien L, Bensimon A, Croquette V. 1997. pH-dependent specific binding and combing of DNA. *Biophys J* **73**: 2064–2070.
- Allemand J-F, Bensimon D, Lavery R, Croquette V. 1998. Stretched and overwound DNA form a Pauling-like structure with exposed bases. *Proc Natl Acad Sci* **95**: 14152–14157.
- Amit R, Gileadi O, Stavans J. 2004. Direct observation of RuvAB-catalyzed branch migration of single Holliday junctions. *Proc Natl Acad Sci* **101**: 11605–11610.
- Avery OT, MacLeod CM, McCarthy M. 1944. Studies on the chemical nature of the substance inducing transformation of pneumococcal types. I. Induction of transformation by a deoxyribonucleic acid fraction isolated from *Pneumococcus* type III. *J Exp Med* **79**: 137–158.
- Berg-Sorensen K, Flyvbjerg H. 2004. Power spectrum analysis for optical tweezers. *Rev Sci Instrum* **75**: 594–612.
- Bouchiat C, Wang M, Block SM, Allemand J-F, Strick T, Croquette V. 1999. Estimating the persistence length of a worm-like chain molecule from force-extension measurements. *Biophys J* **76**: 409–413.
- Bracewell R. 1999. *The Fourier transform and its applications*, 3rd ed. McGraw-Hill, New York.
- Bryant Z, Stone MD, Gore J, Smith SB, Cozzarelli NR, Bustamante C. 2003. Structural transitions and elasticity from torque measurements on DNA. *Nature* **424**: 338–341.
- Bustamante C, Marko J, Siggia E, Smith S. 1994. Entropic elasticity of λ -phage DNA. *Science* **265**: 1599–1600.
- Charvin G, Bensimon D, Croquette V. 2003. Single-molecule study of DNA unlinking by eukaryotic and prokaryotic type-II topoisomerases. *PNAS* **100**: 9820–9825.
- Charvin G, Allemand J-F, Strick TR, Bensimon D, Croquette V. 2004. Twisting DNA: Single molecule studies. *Contemp Phys* **45**: 383–403.
- Charvin G, Strick TR, Bensimon D, Croquette V. 2005a. Topoisomerase IV bends and overtwists DNA upon binding. *Biophys J* **89**: 384–392.
- Charvin G, Vologodskii A, Bensimon D, Croquette V. 2005b. Braiding DNA: Experiments, simulations, and models. *Biophys J* **88**: 4124–4136.
- Chee M, Yang R, Hubbell E, Berno A, Huang X, Stern D, Winkler J, Lockhart DJ, Morris MS, Fodor SPA. 1996. Accessing genetic information with high-density DNA arrays. *Science* **274**: 610–614.
- Danilowicz C, Coljee VW, Bouzigues C, Lubensky DK, Nelson DR, Prentiss M. 2003. DNA unzipped under a constant force exhibits multiple metastable intermediates. *Proc Natl Acad Sci* **100**: 1694–1699.
- Dawid A, Croquette V, Grigoriev M, Heslot F. 2004. Single-molecule study of RuvAB-mediated Holliday-junction migration. *Proc Natl Acad Sci* **101**: 11611–11616.
- Dessinges M-N, Lionnet T, Xi X, Bensimon D, Croquette V. 2004. Single molecule assay reveals strand switching and enhanced processivity of UvrD. *Proc Natl Acad Sci* **101**: 6439–6444.
- Einstein A. 1956. *Investigation of the Brownian theory of movement*, Dover Publications, New York.
- Friese ME, Enger J, Rubinsztein-Dunlop H, Heckenberg NR. 1996. Optical angular-momentum transfer to trapped absorbing particles. *Phys Rev A* **54**: 1593–1596.
- Friese MEJ, Nieminen TA, Heckenberg NR, Rubinsztein-Dunlop H. 1998. Optical alignment and spinning of laser-trapped microscopic particles. *Nature* **394**: 348–350.
- Fulconis R, Bancaud A, Allemand JF, Croquette V, Dutreix M, Viovy JL. 2004. Twisting and untwisting a single DNA molecule covered by RecA protein. *Biophys J* **87**: 2552–2563.
- Gore J, Bryant Z, Stone MD, Nollmann M, Cozzarelli NR, Bustamante C. 2006. Mechanochemical analysis of DNA gyrase using rotor bead tracking. *Nature* **439**: 100–104.
- Gosse C, Croquette V. 2002. Magnetic tweezers: Micro-manipulation and force measurement at the molecular level. *Biophys J* **82**: 3314–3329.
- Hershey A, Chase M. 1952. Independent functions of viral protein and nucleic acid in growth of bacteriophage. *J Gen Physiol* **1**: 39–56.
- Koster DA, Croquette V, Dekker C, Shuman S, Dekker NH. 2005. Friction and torque govern the relaxation of DNA supercoils by eukaryotic topoisomerase IIb. *Nature* **434**: 671–674.
- La Porta A, Wang MD. 2004. Optical torque wrench: Angular trapping, rotation, and torque detection of quartz microparticles. *Phys Rev Lett* **92**: 190801.
- Lee GU, Chrisey LA, Colton RJ. 1994. Direct measurement of the forces between complementary strands of DNA. *Science* **266**: 771–773.
- Leger JF, Romano G, Sarkar A, Robert J, Bourdieu L, Chatenay D, Marko JF. 1999. Structural transitions of a twisted and stretched DNA molecule. *Phys Rev Lett* **83**: 1066–1069.
- Leuba SH, Karymov MA, Tomschik M, Ramjit R, Smith P, Zlatanova J. 2003. Assembly of single chromatin fibers depends on the tension in the DNA molecule: Magnetic tweezers study. *Proc Natl Acad Sci* **100**: 495–500.
- Lia G, Bensimon D, Croquette V, Allemand JF, Dunlap D, Lewis DE, Adhya S, Finzi L. 2003. Supercoiling and denaturation in Gal repressor/heat unstable nucleoid protein (HU)-mediated DNA looping. *Proc Natl Acad Sci* **100**: 11373–11377.
- Lia G, Praly E, Ferreira H, Stockdale C, Tse-Dinh YC, Dunlap D, Croquette V, Bensimon D, Owen-Hughes T. 2006. Direct observation of DNA distortion by the RSC complex. *Mol Cell* **21**: 417–425.
- Lionnet T, Joubaud S, Lavery R, Bensimon D, Croquette V. 2006. Wringing out DNA. *Phys Rev Lett* **96**: 178102.
- Lionnet T, Allemand J-F, Revyakin A, Strick TR, Saleh OA, Bensimon D, Croquette V. 2012. Magnetic trap construction. *Cold Spring Harb Protoc* doi: 10.1101/pdb.prot067496.
- Maier B, Bensimon D, Croquette V. 2000. Replication by a single DNA-polymerase of a stretched single stranded DNA. *Proc Natl Acad Sci* **97**: 12002–12007.
- Marko J, Siggia E. 1995. Stretching DNA. *Macromolecules* **28**: 8759–8770.
- Nieminen TA, Heckenberg NR, Rubinsztein-Dunlop H. 2001. Optical measurement of microscopic torques. *J Mod Optics* **48**: 405–413.
- Ovryn B. 2000. Three-dimensional forward scattering particle image velocimetry applied to a microscopic field-of-view. *Exp Fluids* **29**: S175–S184.

- Ovryn B, Izen SH. 2000. Imaging of transparent spheres through a planar interface using a high-numerical-aperture optical microscope. *J Opt Soc Am A* 17: 1202–1213.
- Press WH, Teukolsky SA, Vetterling WT, Flannery PB. 1992. *Numerical recipes in C: The art of scientific computing*, 2nd ed. Cambridge University Press, London.
- Reif F. 1965. *Fundamentals of statistical and thermal physics*, McGraw-Hill, New York.
- Revyakin A, Allemand JF, Croquette V, Ebright RH, Strick TR. 2003. Single-molecule DNA nanomanipulation: Detection of promoter-unwinding events by RNA polymerase. *Methods Enzymol* 370: 577–598.
- Revyakin A, Ebright RH, Strick TR. 2005. Single-molecule DNA nanomanipulation: Improved resolution through use of shorter DNA fragments. *Nat Methods* 2: 127–138.
- Revyakin A, Liu C, Ebright RH, Strick TR. 2006. Abortive initiation and productive initiation by RNA polymerase involve DNA scrunching. *Science* 314: 1139–1143.
- Saleh OA, Peralis C, Barre FX, Allemand JF. 2004. Fast, DNA-sequence independent translocation by FtsK in a single-molecule experiment. *EMBO J* 23: 2430–2439.
- Saleh OA, Bigot S, Barre FX, Allemand JF. 2005. Analysis of DNA supercoil induction by FtsK indicates translocation without groove-tracking. *Nat Struct Mol Biol* 12: 436–440.
- Sano T, Smith CL, Cantor CR. 1992. Immuno-PCR: Very sensitive antigen detection by means of specific antibody-DNA conjugates. *Science* 258: 120–122.
- Seidel R, van Noort J, van der Scheer C, Bloom JG, Dekker NH, Dutta CF, Blundell A, Robinson T, Firman K, Dekker C. 2004. Real-time observation of DNA translocation by the type I restriction modification enzyme EcoR124I. *Nat Struct Mol Biol* 11: 838–843.
- Shivashankar GV, Feingold M, Krichevsky O, Libchaber A. 1999. RecA polymerization on double-stranded DNA by using single-molecule manipulation: The role of ATP hydrolysis. *Proc Natl Acad Sci* 96: 7916–7921.
- Smith DE, Tans SJ, Smith SB, Grimes S, Anderson DL, Bustamante C. 2001. The bacteriophage straight $\langle gf \rangle 29$ portal motor can package DNA against a large internal force. *Nature* 413: 748–752.
- Smith S, Finzi L, Bustamante C. 1992. Direct mechanical measurements of the elasticity of single DNA molecules by using magnetic beads. *Science* 258: 1122–1126.
- Strick T, Allemand J, Bensimon D, Bensimon A, Croquette V. 1996. The elasticity of a single supercoiled DNA molecule. *Science* 271: 1835–1837.
- Strick T, Allemand J-F, Bensimon D, Croquette V. 1998. The behavior of supercoiled DNA. *Biophys J* 74: 2016–2028.
- Strick T, Bensimon D, Croquette V. 1999. Micro-mechanical measurement of the torsional modulus of DNA. *Genetica* 106: 57–62.
- Strick T, Croquette V, Bensimon D. 2000. Single-molecule analysis of DNA uncoiling by a type II topoisomerase. *Nature* 404: 901–904.
- Watson J, Crick F. 1953a. Genetic implications of the structure of deoxyribonucleic acid. *Nature* 171: 964–967.
- Watson J, Crick F. 1953b. Molecular structure of nucleic acids: A structure for deoxyribose nucleic acid. *Nature* 171: 737–738.
- Yan J, Skoko D, Marko JF. 2004. Near-field-magnetic-tweezer manipulation of single DNA molecules. *Phys Rev E Stat Nonlin Soft Matter Phys* 70: 011905.
- Yang MS, Yau HCM, Chan HL. 1998. Adsorption kinetics and ligand-binding properties of thiol-modified double-stranded DNA on a gold surface. *Langmuir* 14: 6121–6129.